BIOCHEMISTRY
including biophysical chemistry & molecular biology
Article

Biochemistry **2010,** *49,* 443–451 443
DOI: 10.1021/bi9016457

New Glucosidase Inhibitors from an Ayurvedic Herbal Treatment for Type 2 Diabetes: Structures and Inhibition of Human Intestinal Maltase-Glucoamylase with Compounds from *Salacia reticulata*[†]

Lyann Sim,[‡] Kumarasamy Jayakanthan,[§] Sankar Mohan,[§] Ravindranath Nasi,[§] Blair D. Johnston,[§] B. Mario Pinto,*[,§] and David R. Rose*[,‡,∥]

[‡]*Ontario Cancer Institute and Department of Medical Biophysics, University of Toronto, 101 College Street, Toronto, ON, M5G 1L7 Canada,* [§]*Department of Chemistry, Simon Fraser University, 8888 University Drive, Burnaby, BC, V5A 1S6 Canada, and* [∥]*Department of Biology, University of Waterloo, 200 University Avenue West, Waterloo, ON, N2L 3G1 Canada*

Received September 21, 2009

ABSTRACT: An approach to controlling blood glucose levels in individuals with type 2 diabetes is to target α-amylases and intestinal glucosidases using α-glucosidase inhibitors acarbose and miglitol. One of the intestinal glucosidases targeted is the N-terminal catalytic domain of maltase-glucoamylase (ntMGAM), one of the four intestinal glycoside hydrolase 31 enzyme activities responsible for the hydrolysis of terminal starch products into glucose. Here we present the X-ray crystallographic studies of ntMGAM in complex with a new class of α-glucosidase inhibitors derived from natural extracts of *Salacia reticulata,* a plant used traditionally in Ayuverdic medicine for the treatment of type 2 diabetes. Included in these extracts are the active compounds salacinol, kotalanol, and de-O-sulfonated kotalanol. This study reveals that de-O-sulfonated kotalanol is the most potent ntMGAM inhibitor reported to date ($K_i = 0.03$ μM), some 2000-fold better than the compounds currently used in the clinic, and highlights the potential of the salacinol class of inhibitors as future drug candidates.

α-Glucosidase inhibitors make up a class of antihyperglycemic drugs that are often administered to individuals with type 2 diabetes as a way of controlling postprandial glucose levels (*1*−*3*). Such control has been shown to be essential in preventing the progress of impaired glucose tolerance toward type 2 diabetes by decreasing the incidence of hyperglycemia and hyperinsulinemia, thus reducing insulin resistance and stress on the β-cells of the pancreas (*4*). Acarbose (**1**) and miglitol (**2**) (Figure 1) are α-glucosidase inhibitors currently used to control blood glucose levels and work by reversibly inhibiting digestive α-amylases and α-glucosidases (*5*). When taken just prior to a meal, they have an effect of slowing the breakdown of ingested carbohydrates and starches and thus delay absorption of glucose into the bloodstream.

It was generally believed that the carbohydrate mimics containing nitrogen such as acarbose and miglitol are protonated in the active site and act as glycosidase inhibitors because of their ability to mimic the shape and/or charge of the presumed transition state for enzymatic glycoside hydrolysis (*6*).

A relatively new and interesting class of inhibitors consists of the sulfonium ion-containing inhibitors, which were first isolated from *Salacia reticulata*, a plant that is widespread in Sri Lanka and South India and is used in traditional Ayurvedic medicine for treating type 2 diabetes (*7*−*10*). Administration of the herbal extract of *S. reticulata* to rats after a carbohydrate meal significantly reduced blood glucose levels (*11*), and no serious acute toxicity or mutagenicity was observed in rats after the oral ingestion of the extracts at a dose of 5000 mg/kg (*12*). When tested in a double-blind study involving human patients with type 2 diabetes and a placebo control group, the *Salacia* extract was shown to be an effective treatment for type 2 diabetes, with side effects comparable to those of the placebo control group (*13*). In addition, a recent study has also shown that the *Salacia* extract is effective in reducing body weight gain in mice on a normal diet and high-fat diet and could potentially reduce the risk of obesity-associated complications, including type 2 diabetes (*14*).

The active compounds of *S. reticulata* were found to include salacinol (**3**), kotalanol (**4**), and de-O-sulfonated kotalanol (**5**) (*15*−*17*) (Figure 1), whose structures comprise a 1,4-anhydro-4-thio-D-arabinitol core and polyhydroxylated acyclic chain. A special feature of the sulfonium ion inhibitor is the permanent positive charge carried by the sulfur, which is postulated to bind in the same way as a protonated amine inhibitor in the active sites of glucosidases.

Although the discovery and synthesis of novel α-glucosidase inhibitors are important in their own right, it is equally important to study their specific mechanism of inhibition against enzymes

[†]This work was supported by the Canadian Institutes for Health Research (FRN79400) and the Heart and Stroke Foundation of Ontario (NA-6305). L.S. received funding through a postgraduate scholarship from the Natural Sciences and Engineering Research Council of Canada. This work is based upon research conducted at the Cornell High Energy Synchrotron Source (CHESS), which is supported by the National Science Foundation and the National Institutes of Health/National Institute of General Medical Sciences under NSF Grant DMR-0225180, using the Macromolecular Diffraction at CHESS (MacCHESS) facility, which is supported by Grant RR-01646 from the National Institutes of Health, through its National Center for Research Resources.

*To whom correspondence should be addressed. E-mail: drrose@scimail.uwaterloo.ca (D.R.R.) or bpinto@sfu.ca (B.M.P.).

Published on Web 12/29/2009

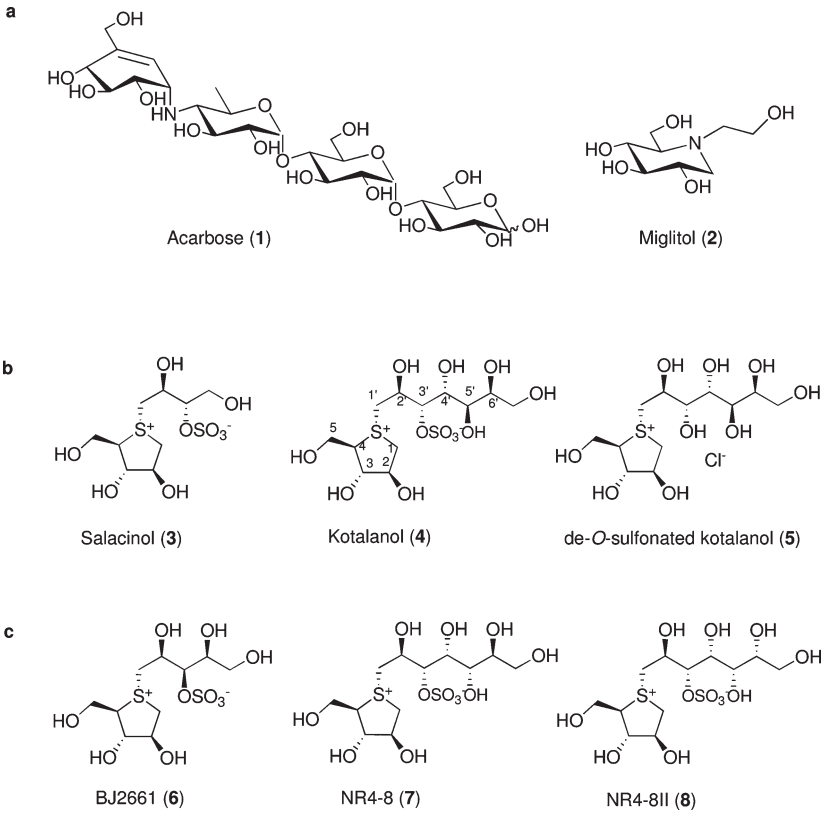

FIGURE 1: α-Glucosidase inhibitors discussed in this paper. (a) Structures of α-glucosidase inhibitors currently used in the treatment of type 2 diabetes: acarbose (**1**) and miglitol (**2**). (b) Structures of the active compounds from *Salacia reticulata*: salacinol (**3**), kotalanol (**4**), and de-O-sulfonated kotalanol (**5**). (c) Side chain derivatives of salacinol: BJ2661 (**6**), NR4-8 (**7**), and NR4-8II (**8**).

involved in carbohydrate digestion. In humans, family GH31[1] glycoside hydrolases maltase-glucoamylase (MGAM) and sucrase-isomaltase (SI) are responsible for the digestion of terminal starch products left after α-amylase action. These membrane-bound enzymes contain two catalytic subunits: an N-terminal subunit (ntMGAM and ntSI) that is proximal to the membrane-bound end and a C-terminal luminal subunit (ctMGAM and ctSI). The substrate specificities of the catalytic subunits vary and overlap to include maltose, isomaltose, sucrose, and small linear and branched oligosaccharides (*18*, *19*).

In our previous studies (*20*−*22*), we had shown that the best inhibitors belonging to the salacinol class have K_i values in the low micromolar range (i.e., 0.10−0.19 μM) and are better inhibitors of ntMGAM compared to acarbose (K_i = 62 μM). The salacinol inhibitors are selective against the intestinal glucosidases as they have been shown to be relatively poor inhibitors of human pancreatic α-amylase (K_i = 75 μM) (*22*), a family 13 endohydrolase responsible for degrading starch into shorter linear and branched oligosaccharides. In contrast, α-amylase is inhibited more strongly by acarbose (K_i = 15 nM) (*23*). Miglitol is similar to the salacinol compounds in that it selectively targets intestinal glucosidases and is a poor inhibitor of α-amylases (*24*). Since the digestive enzymes targeted by α-glucosidase inhibitors vary in substrate specificity for different carbohydrate structures, some studies have suggested that the efficacy of the inhibitors is dependent on the carbohydrate diet profile of the individual (*25*−*27*). These results suggest that a multitarget, combination therapy approach might be beneficial.

In recent studies, we have determined the crystal structure of ntMGAM in complex with acarbose and proposed the structural basis for its poor inhibitory properties (*28*). Here, we present the crystal structures of ntMGAM in complex with miglitol and salacinol and compare their mechanisms of inhibition to that of acarbose. We also present crystal complex structures of kotalanol, de-O-sulfonated kotalanol, and several salacinol derivatives, including BJ2661 (**6**), NR4-8 (**7**), and NR4-8II (**8**), to study the essential structural features of this class of inhibitors and their effect on function. These insights provide a strong foundation for the development of more effective α-glucosidase inhibitors for controlling blood glucose levels.

The results are relevant to "alternative" therapies, which are often hampered by a lack of understanding of their mode of action at the molecular level. The classical approach to clinical compounds is to identify likely target activities and screen or design compounds to intervene. However, this can lead to unexpected complications in synthesis, bioavailability, and toxicity, which makes that approach very costly in developing pharmaceuticals. The alternative approach used here starts with a traditional treatment that shows clinical effectiveness and is, therefore, already a validated activity. Identification of the active principles together with an understanding of their mechanism of action can lead, in turn, to acceptance of the alternative therapy.

MATERIALS AND METHODS

Inhibitors. All compounds from the salacinol class of inhibitors examined in this paper (Figure 1) were synthesized by the

[1]Abbreviations: GH31, family 31 glycoside hydrolase; MGAM, maltase-glucoamylase; SI, sucrase-isomaltase; ntMGAM, N-terminal subunit of MGAM; ntSI, N-terminal subunit of SI; ctMGAM, C-terminal subunit of MGAM; ctSI, C-terminal subunit of SI; rmsd, root-mean-square deviation.

Table 1: Data Collection and Refinement Statistics

	miglitol	salacinol	BJ2661	kotalanol	de-O-sulfonated kotalanol
PDB code	3L4W	3L4Z	3L4T	3L4V	3L4U
			Crystal Parameters		
space group	$P2_12_12_1$	$P2_12_12_1$	$P2_12_12_1$	$P2_12_12_1$	$P2_12_12_1$
unit cell dimensions (Å)					
a	93.7	92.4	92.8	91.3	88.9
b	107.9	108.8	108.4	109.7	109.9
c	111.8	111.1	110.8	110.1	109.8
			Data Collection[a]		
no. of unique reflections	76058	75286	85496	65399	84175
redundancy	7.4 (5.6)	7.7 (6.6)	6.4 (5.1)	7.3 (7.4)	7 (6.7)
$I/\sigma I$	9.6 (3.1)	15.2 (4.0)	18.3 (3.0)	13.9 (3.5)	14.1 (3.4)
completeness (%)	96.5 (83.6)	99.1 (99.5)	95.8 (84.8)	99.9 (100)	99.9 (10)
R_{sym} (%)	11.9 (54.3)	10.3 (49.8)	8.5 (53.8)	12.2 (51.5)	12.1 (60.8)
			Refinement		
R/R_{free} (%)	19.8 (23.2)	20.3 (25.3)	25.2 (29.1)	18.2 (23.1)	18.5 (22.0)
resolution range (Å)	20−2.0	20−2.0	20−1.9	20−2.1	20−1.9
rmsd for bonds (Å)	0.014	0.016	0.015	0.015	0.016
rmsd for angles (deg)	1.57	1.62	1.57	1.58	1.58
average protein *B*-factor (Å^2)	29.1	33.6	27.8	25.6	20.8
average ligand *B*-factor (Å^2)	24.8	38.3	30.6	26.4	22.3

[a]Values in parentheses refer to the highest-resolution shell.

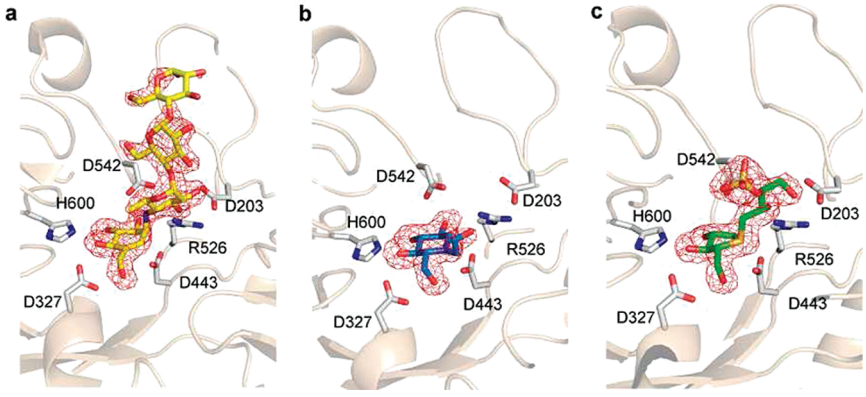

FIGURE 2: ntMGAM active site with bound inhibitors: (a) acarbose (yellow), (b) miglitol (blue), and (c) salacinol (green). $F_o - F_c$ electron density maps (red), with the inhibitor omitted from the calculation, are contoured at 2.3σ, 3.0σ, and 3.0σ, respectively. Representative active site residues are shown as gray sticks and include the catalytic nucleophile D443 and acid/base catalyst D542.

Pinto laboratory (*29*−*31*), and miglitol was purchased from Toronto Research Chemicals Inc. (North York, ON).

Crystallization and Inhibitor Soaks. ntMGAM overexpression in *Drosophila* S2 cells, purification, and modification via reductive methylation were previously described by Sim et al. (*28*). ntMGAM crystals were grown in a hanging drop diffusion experiment using 1 μL of protein (~10 mg/mL) and 1 μL of reservoir buffer (200 mM sodium sulfate and 20% PEG 3350). We obtained inhibitor complexes by soaking crystals in mother liquor supplemented with 200 μM inhibitor for ~1−12 h and then cryoprotecting them with 20% glycerol, 200 mM sodium sulfate, and 20% PEG 3350 before they were flash-frozen in liquid nitrogen.

Data Collection, Processing, and Refinement. Data for the ntMGAM crystal complexes were collected on an ADSC Quantum-270 CCD detector at beamline F1 at the Cornell High Energy Synchrotron Source (CHESS) and were processed with HKL2000 (*32*). Data collection statistics are summarized in Table 1 and in Table 1 of the Supporting Information.

It was observed from these and previous experiments (*28*) that two ntMGAM crystal forms exist and appear at equal frequencies. The crystals described in this paper were isomorphous either to the determined native ntMGAM structure [Protein Data Bank (PDB) entry 2QLY] or to the ntMGAM−acarbose structure (PDB entry 2QMJ), which differ slightly in unit cell dimensions (*28*). The native ntMGAM structure was used as an initial starting model for the refinement of the salacinol, miglitol, kotalanol, and BJ2661 data sets, whereas the ntMGAM−acarbose structure (with acarbose removed) was used as an initial starting model for refinement of the de-O-sulfonated kotalanol, NR4-8, and NR4-8II data sets. Following several alternating cycles of restrained refinement using REFMAC (*33*) and manual fitting using Coot (*34*), $F_o - F_c$ maps clearly revealed the position of the bound inhibitors in the ntMGAM active site (Figures 2 and 5 and Figure 1 of the Supporting Information). Inhibitor topologies and restraints were generated using the PRODRG server (*35*), and water

molecules were picked using Arp/Warp (*36*). A summary of the refinement statistics is given in Table 1 and in Table 1 of the Supporting Information. Protein superposition for the comparison of active site residues and inhibitor binding were conducted using the "align Cα" function in Pymol. Graphics were generated using Pymol (http://pymol.sourceforge.net) and ChemDraw.

Inhibition Assays. Inhibition assays of ntMGAM with acarbose, salacinol, and salacinol derivatives have been described previously (*20*, *37*). Apart from a few modifications to the protocol as outlined below, the inhibition assays with miglitol, BJ2661, kotalanol, de-O-sulfonated kotalanol, NR4-8, and NR4-8II were performed in a manner similar to those with the previous inhibitors. Analysis of ntMGAM inhibition was performed using a two-step assay, which entailed reaction of ntMGAM with maltose, quenching of the reaction, and reaction with glucose oxidase (Sigma-Aldrich) to quantify the amount of glucose released. Assays were conducted in 96-well microtiter plates containing 100 mM MES buffer (pH 6.5), an inhibitor (at three different concentrations), maltose as a substrate (2.5, 3.5, 5, 7.5, 15, and 30 mM), and 2 nM ntMGAM, with a final volume of 50 μL. Reaction mixtures were incubated at 37 °C for 30 min and reactions terminated with Tris-HCl (pH 7) to a final concentration of 1 M. Aliquots of glucose oxidase reagent (125 μL) were added to each well and left to develop at 37 °C for 30 min. Absorbance was measured at 450 nm and compared to a standard glucose curve to determine the amount of glucose produced by ntMGAM activity in the reaction. All reactions were performed in triplicate, and absorbance measurements were averaged to give a final result. In previous experiments (*20*), boiling was used to stop the ntMGAM reaction. However, we found that quenching with Tris-HCl was easier and allowed us to conduct the full two-step reaction in microtiter plates.

RESULTS

ntMGAM Inhibition by Three Different Classes of α-Glucosidase Inhibitors. (*i*) *ntMGAM−Acarbose Structure*. Insights into the poor inhibitory property of acarbose against ntMGAM were revealed in the crystal structure of the ntMGAM−acarbose complex determined to 1.9 Å resolution (PDB entry 2QMJ) (*28*). The structure showed that the ntMGAM substrate-binding site consisted of a −1 and a +1 sugar-binding site, which in the inhibitor complex structure is occupied by the two nonreducing rings of acarbose (acarvosine rings) (Figure 2a). Main interactions include hydrogen bonding of the acarvosine ring hydroxyl groups to the side chains of D327, H600, D542, R526, and D203 (Figure 3a). The two remaining rings, from the reducing end of acarbose, make almost no interactions with ntMGAM, and the ring atoms have higher ring *B*-factors (*28*).

(*ii*) *ntMGAM−Miglitol Structure*. Miglitol, a selective inhibitor of intestinal glucosidases and considered a poor inhibitor of α-amylases (*24*), was found to inhibit ntMGAM with a K_i of 1.0 μM (Table 2). The crystals of ntMGAM soaked in 200 μM miglitol diffracted to 2.0 Å, and $F_o - F_c$ maps, calculated with apo-ntMGAM as a model, clearly revealed miglitol binding in the active site (Figure 2b). Miglitol is a much smaller inhibitor compared to acarbose and occupies only the −1 subsite of ntMGAM. Similar to acarbose, miglitol interacts with ntMGAM mainly through hydrogen bonding interactions with D327, H600, and D542 side chains but lacks the D203 and R526 interactions as the inhibitor does not extend toward the +1 site (Figure 3b).

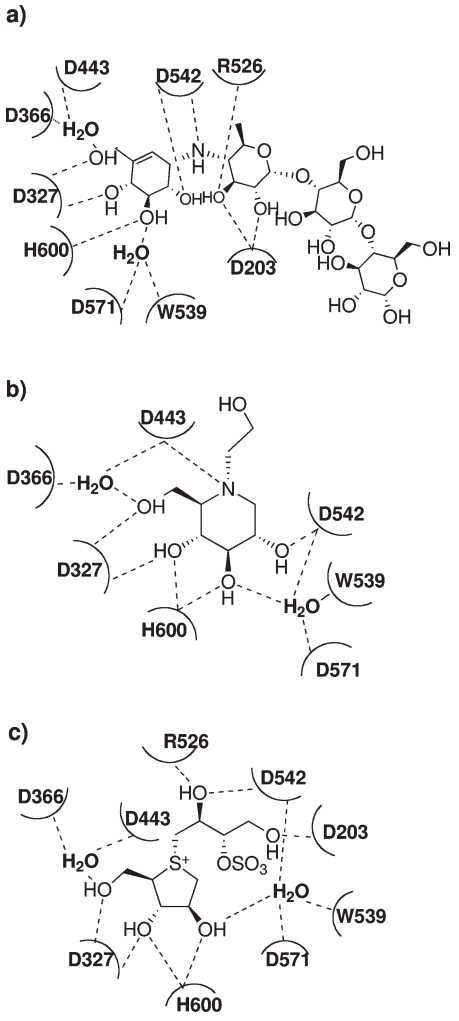

FIGURE 3: ntMGAM−inhibitor interactions. Schematic representation of interactions (dotted lines) between the ntMGAM side chain residues (half-circles) and (a) acarbose, (b) miglitol, and (c) salacinol.

The hydroxyl group of the *N*-hydroxyethyl chain also does not contribute to any significant interactions with ntMGAM. However, the ring nitrogen of miglitol is within hydrogen bonding distance (2.8 Å) of the catalytic nucleophile D443.

(*iii*) *ntMGAM−Salacinol Structure*. Members of the zwitterionic family of compounds, which includes salacinol, are potent inhibitors of ntMGAM (for a review, see ref *22*). Salacinol, the parent compound of all the derivatives described in this paper, inhibits ntMGAM with a K_i of 0.19 μM (Table 2). Crystals of ntMGAM soaked in 200 μM salacinol diffracted to 2.0 Å, and $F_o - F_c$ maps, calculated with apo-ntMGAM as a model, clearly revealed salacinol binding in the active site (Figure 2c). Compared to miglitol, salacinol is a slightly larger inhibitor, occupying the −1 and +1 ntMGAM subsites. In the −1 subsite, interactions are between the ring hydroxyl groups of salacinol and ntMGAM side chains D327 and H600. There is an additional electrostatic interaction between the sulfonium ion center of salacinol and the catalytic nucleophile D443, which is 3.2 Å away. In the +1 subsite, the hydroxyl groups of the acyclic chain of salacinol form hydrogen bonds with the side chains of D203, R526, and the acid/base catalyst D542 (Figure 3c). The sulfate group of the acyclic chain does not make direct contact with any subsite residues but is instead exposed at the opening of the pocket.

Acarbose, miglitol, and salacinol all form hydrogen bonds with two active site water molecules which are tightly bound via

Table 2: Inhibition of ntMGAM by α-Glucosidase Inhibitors

		stereochemistry at the stereogenic centers in the acyclic side chains					reference (enzyme kinetics)
inhibitor	K_i (μM)	C2′	C3′	C4′	C5′	C6′	
acarbose	62 ± 13	–	–	–	–	–	*20*
miglitol	1.0 ± 0.1	–	–	–	–	–	this report
salacinol	0.19 ± 0.02	*S*	*S*	–	–	–	*20*
BJ2661	3.8 ± 0.8	*S*	*R*	*S*	–	–	this report
NR4-8	0.13 ± 0.02	*S*	*S*	*R*	*S*	*S*	*21*
NR4-8II	0.10 ± 0.02	*S*	*S*	*R*	*S*	*R*	*21*
kotalanol	0.19 ± 0.03	*S*	*S*	*R*	*R*	*S*	this report
de-O-sulfonated kotalanol	0.03 ± 0.01	*S*	*S*	*R*	*R*	*S*	this report

hydrogen bonding to D366, D443, D571, and W539 (Figure 3). The −1 pocket of ntMGAM is also lined with bulky hydrophobic groups that likely contribute to stacking interactions and the orientation of sugar rings (*28*).

(*iv*) *Comparison of ntMGAM−Inhibitor Structures*. The acarbose, miglitol, and salacinol inhibitors described in this section differ in many ways, including charge, ring structure, size, and their ability to inhibit ntMGAM. Acarbose, the largest inhibitor of the three, inhibited ntMGAM the least. It was proposed from previous studies that the poor inhibition of ntMGAM by acarbose was due to its lack of an extended sugar binding site (+2 and +3) and thus an inability to bind to the sugar rings of acarbose (*28*). In conjunction with sequence comparison and kinetic studies, it was then suggested that the C-terminal subunit of MGAM (ctMGAM) likely contains an extended sugar binding site, which might explain why it is very strongly inhibited by acarbose (*28*, *38*).

Compared to acarbose, miglitol and salacinol are much smaller compounds and are ~60- and ~300-fold better inhibitors of ntMGAM, respectively. Since they do not require additional interactions with +2 and +3 subsites to make them better inhibitors, which is needed for acarbose, the miglitol and salacinol structures likely possess features not present in the acarvosine ring, which account for tighter binding to the −1 and +1 subsites.

To compare how acarbose, salacinol, and miglitol bind to the −1 and +1 subsites, the active sites of the three structures were superimposed (Figure 4a). In the −1 subsite, there is a relatively good global overlap of the miglitol and acarbose−valienamine rings and their C2, C3, C4, and C6 hydroxyl groups. Salacinol is a five-membered ring; thus, its C2, C3, and C5 ring hydroxyl groups overlap with the C3, C4, and C6 hydroxyl groups of the six-membered ring inhibitors. Beyond the −1 site, the inhibitors do not share any similarity in binding. Miglitol, the smallest inhibitor of the three, binds solely to the −1 subsite. Its *N*-hydroxyethyl arm does not make any interactions with ntMGAM and instead protrudes into the side of the active site pocket and enlarges it by shifting a tryptophan side chain (W406) by 0.4−2.4 Å (Figure 4a). The enlargement of the active site pocket likely induces the active site methionine (M444) to generate alternative side chain conformations to fill the void space left by W406 (Figure 4a). Other differences include a shift in catalytic nucleophile D443 of ~0.4 Å and a shift in acid/base catalyst D542 of 0.4−0.6 Å, compared to the other two inhibitor structures. Other than these changes, there is structural conservation for the rest of the active site residues in the −1 subsite.

In the +1 subsite, the acarbose ring and acyclic chain of salacinol do not superimpose. However, the R526, D203, and

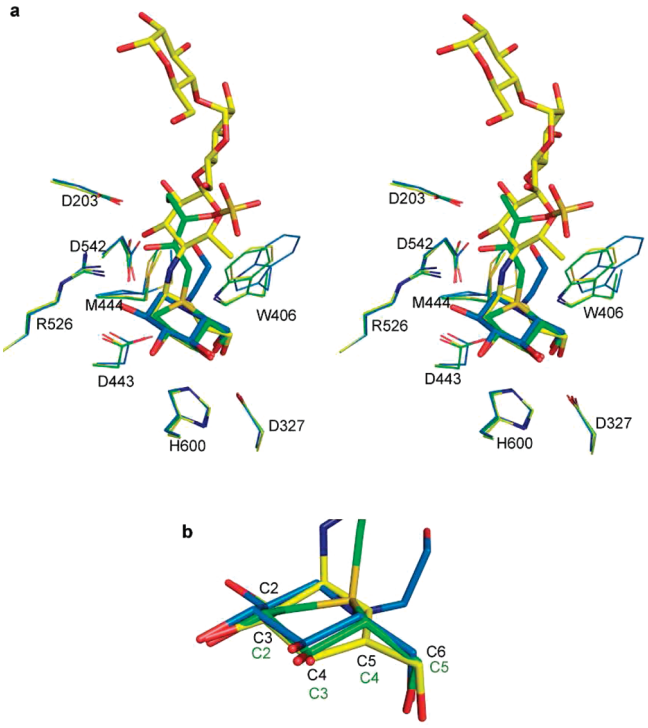

FIGURE 4: (a) Comparison of ntMGAM−inhibitor active sites. Shown is a stereodiagram (divergent) of the superimposed active sites of ntMGAM−acarbose (yellow), ntMGAM−miglitol (blue), and ntMGAM−salacinol (green) structures. Thick and thin lines of the same color are used to represent bound inhibitors and interacting residues, respectively. (b) Comparison of inhibitors binding to the −1 subsite. Superimposed carbon ring atoms of miglitol and acarbose are numbered in black and those of salacinol in green.

D542 ntMGAM−acarbose and ntMGAM−salacinol residues interacting with the hydroxyl groups superimpose very well. Both the salacinol C4′ hydroxyl group and the C2 acarbose hydroxyl group form a hydrogen bond to D203. However, the C2′ hydroxyl group of the salacinol acyclic chain is positioned in a manner such that hydrogen bonds are made with both D542 and R526 (2.5 and 2.7 Å, respectively) compared to the C3 hydroxyl group of the acarbose ring, which interacts with only R526 (2.8 Å) (Figures 3a,c and 4a).

An important difference between the binding of the three inhibitors is in the ring conformation adopted in the −1 subsite (Figure 4b). From structural studies of a GH31 xylosidase, it was proposed that the reaction mechanism, from substrate binding through the putative transition state to formation of a covalent enzyme−substrate intermediate, proceeds through a $^4C_1-^4H_3-^1S_3$ conformational itinerary for this family (*39*).

In the ntMGAM−miglitol structure, miglitol adopts a $^4C_1$ structure and thus does not mimic the charged oxacarbenium ion-like transition state but instead is similar to the proposed substrate-binding conformation. In comparison, salacinol adopts a $^3T_2$ conformation in the ntMGAM active site, the same conformation that its native unbound state adopts (*40*). If one aligns C2, C3, and C4 of the salacinol ring with C3, C4, and C5, respectively, of a glucopyranose ring, the $^3T_2$ conformation of the salacinol ring closely resembles the $^4H_3$ conformation of the proposed transition state. In addition, the electrostatic interaction between the sulfonium ion center and D443 does mimic that between the positively charged oxacarbenium ion transition state and the active site carboxylate in the hydrolysis.

Unlike miglitol and salacinol, which both mimic a state in the proposed conformational itinerary, the valienamine ring of acarbose adopts a $^2H_3$ half-chair conformation. The lack of similarity of the valienamine ring structure to any of the reaction mechanism conformations provides an explanation for the poor inhibition of ntMGAM by acarbose. The $^2H_3$ conformation has an effect on the positioning of C3, C4, and C5 of the acarbose valienamine ring, thus shifting their corresponding OH or CH_2OH groups (Figure 4b). Since these hydroxyl groups play a large role in hydrogen bonding, a slight shift in angle or positioning is likely to affect binding.

Whether acarbose is a true transition-state analogue or simply a tight binder is also a topic of debate (*41*, *42*). Although the $^2H_3$ half-chair conformation of acarbose is a conformation not likely adopted by an oxacarbenium ion-like transition state (*41*), extensive kinetic studies on active site mutants of cyclodextrin glucanotransferase belonging to the GH13 family have shown acarbose to be a good transition-state analogue (*43*). However, similar studies conducted on an inverting glucoamylase from the GH15 family suggested that acarbose is a poor transition-state mimic in that system (*44*). The extents to which acarbose, salacinol, and miglitol are transition-state mimics of GH31 enzymes will require further kinetic studies on active site mutants.

Since it is suggested that additional subsite interactions with the acarbose sugar rings would significantly enhance its inhibitory properties (*28*, *38*), it would be of interest to see whether extending the salacinol or miglitol inhibitors into the +2 or +3 subsites would increase their inhibitory properties in enzymes with extended sugar binding sites such as ctMGAM. Salacinol derivatives with extended acyclic chains have been synthesized and have exhibited inhibitory properties similar to those of salacinol against ntMGAM (*21*).

Replacement of the *N*-hydroxyethyl group of miglitol with the acyclic chain of salacinol was shown to decrease inhibitor potency (*20*). As the *N*-hydroxyethyl group of miglitol was shown to displace some active site residues instead of extending into the +1 site of ntMGAM (Figure 4a), modification to this group would not be beneficial in making interactions with additional subsites.

Inhibition of ntMGAM by Salacinol Derivatives. (*i*) *Inhibitory Structural Elements of Salacinol Derivatives*. In recent years, there have been a large number of reports describing the synthesis of salacinol derivatives and the evaluation of their inhibitory activities (for a review, see ref *22*). Most recently, Jayakanthan et al. (*30*) described the synthesis and structure conformation of kotalanol and its de-O-sulfonated analogue (Figure 1), two active compounds from *S. reticulata* that have extended acyclic chains compared to salacinol. Here, we investigate how the length of the acyclic polyhydroxylated chain, stereochemistry, and presence of the sulfate group affect the binding of the salacinol derivatives to the ntMGAM site. From previous synthetic and kinetic studies, which involved the systematic evaluation of the effect of different chain lengths as well as different stereochemistries at the stereogenic centers on ntMGAM activity (*20*, *37*, *29*, *45*, *46*), it was possible to draw the following conclusions. (1) An *S* configuration at the C2′ center and an *R* configuration at the C4′ center are critical for effective inhibition. (2) Sulfate stereochemistry at C3′ is not important. (3) Acyclic chains longer than four carbons do not significantly enhance the inhibitory properties.

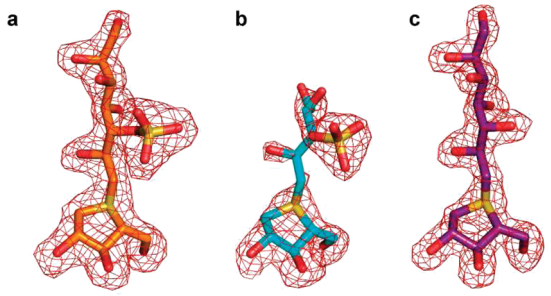

FIGURE 5: Electron density of salacinol derivatives in the ntMGAM active site. Shown are the $F_o - F_c$ maps calculated for the (a) kotalanol (orange), (b) BJ2661 (cyan), and (c) de-O-sulfonated kotalanol (purple) structures, with inhibitors omitted from the calculations. Maps are contoured at 2.3σ.

To demonstrate the structural basis for these observations, selected salacinol derivatives differing in acyclic chain length, stereoconfiguration, and the presence of a sulfate group were soaked into ntMGAM crystals. Inhibition constants and acyclic chain stereochemistries of the salacinol derivatives are summarized in Figure 1 and Table 2.

(*ii*) *Effect of an Extended Acyclic Chain on ntMGAM Inhibition*. The effects of an extended acyclic hydroxyl chain on inhibitor binding were examined by comparing the salacinol, kotalanol, NR4-8, and NR4-8II structures. Compared to the four-carbon side chain of salacinol, kotalanol has an extended seven-carbon polyhydroxylated side chain with *S*, *S*, *R*, *R*, and *S* stereoconfigurations at C2′, C3′, C4′, C5′, and C6′, respectively. The structure of ntMGAM in complex with kotalanol was determined to 2.1 Å, and the electron density is well-defined for the bound inhibitor (Figure 5a). The ntMGAM active sites in the kotalanol and salacinol complexes are structurally conserved, and the inhibitors superimpose identically, except for the C4′−C7′ OH substituents that are absent in salacinol (Figure 6a). The extended chain makes a few additional contacts with ntMGAM through hydrogen bonding between the C6′ OH group and the side chain of D203 and through water interactions between C5′−C7′ hydroxyls and residues D203 and T205 (Figure 6a). These additional interactions do not seem to improve or hinder the binding of kotalanol, as its inhibition constant ($K_i = 0.19$ μM) is identical to that of salacinol ($K_i = 0.19$ μM). Moreover, kotalanol analogues NR4-8 and NR4-8II (Figure 1), which have *S*,*S* and *S*, *R* configurations at C5′ and C6′, respectively, also exhibit similar strong inhibition constants (K_i = 0.13 and 0.10 μM, respectively) (*21*). In the crystal structure of NR4-8 and NR4-8II bound to ntMGAM, the C5′−C7′ arm of NR4-8 is disordered whereas that of NR4-8II binds in a different conformation compared to that of kotalanol (Figures 1 and 2 of the Supporting Information). This is additional evidence that the binding conformation of the C5′−C7′ arm does not contribute significantly to the inhibitory properties of the compound against ntMGAM.

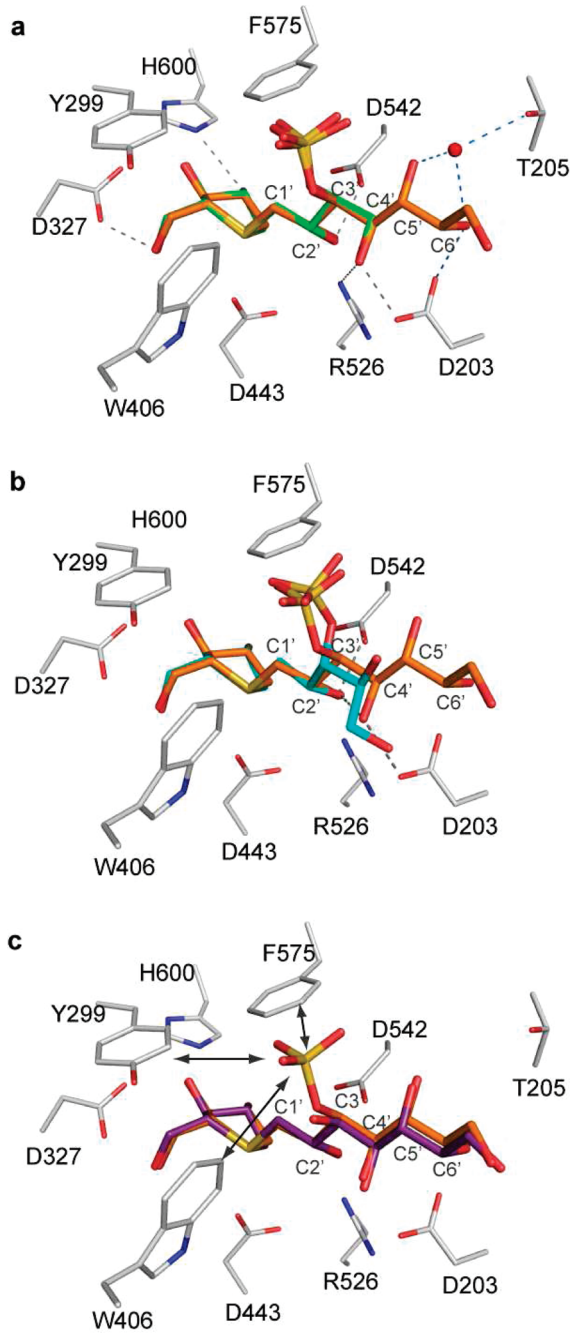

FIGURE 6: Superposition of salacinol and salacinol derivatives in the ntMGAM active site. Active site residues for all ntMGAM structures superimpose; however, for the sake of clarity, only one set of residues is shown. The stereocenters of the acyclic chain of kotalanol are labeled C1′−C6′. (a) Superposition of salacinol (green) and kotalanol (orange) structures. Common hydrogen bonding interactions are shown as gray dashes, and additional hydrogen bonding by the C5′−C7′ OH groups of kotalanol is shown as blue dashes. (b) Superposition of kotalanol (orange) and BJ2661 (cyan) structures. The hydrogen bonding interaction between ntMGAM and kotalanol groups through D203, the C4′ OH group, the C2′ OH group, and D542 is shown as gray dashes. (c) Superposition of kotalanol (orange) and de-O-sulfonated kotalanol (purple) structures. Double-headed arrows show the proximities of the sulfate group to the surrounding hydrophobic residues Y299, W406, and F575, which are 3.5, 3.9, and 3.9 Å, respectively, from the group.

(*iii*) *Effect of Chain Stereoconfiguration on ntMGAM Inhibition*. When soaked into ntMGAM crystals, derivatives with ring stereoconfigurations deviating from those of salacinol or derivatives with an *R* configuration at the C2′ OH group could not be seen in the active site, demonstrating the importance of these groups in inhibitor binding. From inhibition studies, an *R* configuration at C4′ was also deemed important in binding, but not as crucial as that at the C2′ position, as we were able to soak BJ2661 (K_i = 3.8 μM), an inhibitor with an *S* configuration at C4′, into ntMGAM crystals. The structure of the ntMGAM complex with BJ2661, containing a five-carbon acyclic chain with stereoconfigurations *S*, *R*, and *S* at C2′, C3′, and C4′, respectively, was determined to 1.9 Å and reveals broken density in the active site (Figure 5b). In contrast to the well-defined electron density of kotalanol (Figure 5a) and de-O-sulfonated kotalanol (Figure 5c), the density surrounding BJ2661 is broken between C1′ and C3′ and is less resolved for the ring C1 and acyclic chain hydroxyl groups at C4′ and C5′. The poor density surrounding BJ2661 suggests weaker binding to ntMGAM and agrees with the inhibition kinetics (Table 2).

Superposition of BJ2661 and kotalanol structures reveals structural conservation of the ntMGAM active site (data not shown) and alignment of the inhibitor ring structures up to the C2′ OH group (Figure 6b). The stereogenic center at C3′ in BJ2661 deviates from that of kotalanol. However, the sulfate groups in both structures are positioned similarly and point toward the exterior of the active site. The sulfate group does not make any significant hydrogen bonding interactions with the ntMGAM active site but seems to be constrained by the bulky hydrophobic groups Y299, W406, and F575, which are 3.5, 3.9, and 3.9 Å, respectively, from the sulfate group (Figure 6c).

In addition to its role in forming a hydrogen bond to D203, the C4′ OH group seems to have an important role in stabilizing the orientation of the C2′ hydroxyl group, via internal hydrogen bonding. The C4′ OH−C2′ OH interaction is present in the salacinol, kotalanol, and de-O-sulfonated kotalanol structures, all of which have *R* configurations at C4′ (Figure 6b). However, due to the *S* configuration at C4′ in BJ2661, which reorients the hydroxyl group and eliminates hydrogen bonding interactions with D203, the stabilizing interaction that goes from D203 to the C4′ OH group to the C2′ OH group is not present in the BJ2661 structure. This may explain why there is a breakage in electron density observed between C1′ and C3′ as the missing interaction is required to stabilize this region of the inhibitor.

(*iv*) *Effect of De-O-sulfonation on ntMGAM Inhibition*. With a K_i of 0.03 μM, the de-O-sulfonated version of kotalanol is the strongest inhibitor of ntMGAM reported thus far. It is interesting to note that changing the sulfate stereoconfiguration at C3′ does not impact the inhibition (*22*), but removing the sulfate group enhances the inhibitory activity of the compound by approximately 7-fold. The structures of kotalanol and its de-O-sulfonated analogue, determined to 1.9 Å, were compared to determine the effect of removing the sulfate group on inhibitor binding (Figure 6c). The two inhibitors overlap until the C3′ group, after which the acyclic chains diverge slightly from one another. Without the bulky sulfate group, the C3′ OH group in de-O-sulfonated kotalanol is repositioned ~0.3 Å closer to the CH_2 group of W406. There is also a 0.3 Å shift between the C4′ OH groups. It is possible that via removal of the sulfate group, the positional constraint imposed by the bulky hydrophobic residues surrounding the C3′ group is relieved, allowing the rest of the polyhydroxylated chain to make optimal contacts with the ntMGAM active site.

DISCUSSION

From the crystal structures of ntMGAM−salacinol derivative complexes, we have identified several key structural elements in salacinol-based compounds required for effective inhibition. First, we observed that the extended hydroxylated side chain of kotalanol, NR4-8, and NR4-8II either is disordered or displays different binding configurations at the C5′−C7′ groups (Figure 6a and Figures 1 and 2 of the Supporting Information). Moreover, the extended chain does not make any significant interactions with the ntMGAM binding site and thus does not add to or hinder its inhibitory properties. Second, an appreciation has been gained of why the absolute stereochemical configurations at C2′ and C4′ must be conserved for tight inhibitor binding. The C2′ OH group makes important hydrogen bonding contacts with R526 and D542 (Figures 3 and 6b), but without the supporting interactions generated by the C4′ OH group, which in turn is held in place by D203, it becomes more disordered, as seen in the BJ2661 electron density (Figure 5b). Third, the BJ2661 and kotalanol sulfate groups align well despite having opposite C3′ stereoconfigurations. Finally, removal of the sulfate group enhances inhibitory activity and slightly affects the conformation of the rest of the polyhydroxylated chain. We conclude that although the stereoconfiguration at C3′ does not affect inhibitory activity, the proximity of the sulfate group to the large hydrophobic groups (Y299, W406, and F575) likely restricts its conformational freedom.

The structural analysis of the inhibitor complexes discussed in this paper has also revealed interesting features relating to the binding mechanism of several classes of α-glucosidase inhibitors, two of which are currently used in the treatment of type 2 diabetes. From inhibition kinetics, we have determined that de-O-sulfonated kotalanol from the salacinol class of compounds is an ∼30-fold stronger inhibitor compared to miglitol and an ∼2000-fold stronger inhibitor compared to acarbose. Comparing the binding mechanisms of acarbose, miglitol, and salacinol has shown the potential of the salacinol class of inhibitors as future drug candidates. Since acarbose and salacinol compounds display complementary inhibition toward starch-digesting enzymes, we suggest that there would be a benefit to the introduction of the latter in combination drug therapy to control blood glucose levels under varying prandial and physical conditions. Moreover, the salacinol-based compounds were shown to be more effective inhibitors of ntMGAM compared to miglitol. This may improve the selective targeting of intestinal glucosidases, which has been thought to help reduce some gastrointestinal side effects associated with acarbose treatment (*47*). Finally, the structures of several salacinol derivatives bound to ntMGAM have highlighted the structural features that are important for effective inhibition that were predicted from previous kinetic studies. Such information can be used to advantage in the design of the next-generation inhibitors.

SUPPORTING INFORMATION AVAILABLE

Data collection and refinement statistics for the ntMGAM−NR4-8 and −NR4-8II complexes (PDB 3L4X and 3L4Y, respectively) and Figures 1 and 2 for these compounds. This material is available free of charge via the Internet at http://pubs.acs.org.

REFERENCES

1. Holman, R. R., Cull, C. A., and Turner, R. C. (1999) A randomized double-blind trial of acarbose in type 2 diabetes shows improved glycemic control over 3 years (U.K. Prospective Diabetes Study 44). *Diabetes Care 22*, 960–964.
2. Krentz, A. J., and Bailey, C. J. (2005) Oral antidiabetic agents: Current role in type 2 diabetes mellitus. *Drugs 65*, 385–411.
3. Mooradian, A. D., and Thurman, J. E. (1999) Drug therapy of postprandial hyperglycaemia. *Drugs 57*, 19–29.
4. Scheen, A. J. (2003) Is there a role for α-glucosidase inhibitors in the prevention of type 2 diabetes mellitus? *Drugs 63*, 933–951.
5. Asano, N. (2003) Glycosidase inhibitors: Update and perspectives on practical use. *Glycobiology 13*, 93–104.
6. Stuttz, A. E. (1999) Iminosugars as glycosidase inhibitors: Nojirimycin and beyond, Wiley-VCH, Weinheim, Germany.
7. Chandrasena, J. P. C. (1935) The Chemistry and Pharmacology of Ceylon and Indian Medicinal Plants, H&C Press, Colombo, Sri Lanka.
8. Jayaweera, D. M. A. (1981) Medicinal Plants Used in Ceylon-Part 1, National Science Council of Sri Lanka, Colombo, Sri Lanka.
9. Vaidyartanam, P. S. (1993) in Indian Medicinal Plants: A compendium of 500 species (Warrier, P. K., Nambiar, V. P. K., and Ramankutty, C., Eds.) Orient Longman, Madras, India.
10. Matsuda, H., Yoshikawa, M., morikawa, T., Tanabe, G., and Muraoka, O. (2005) Antidiabetogenic constituents from *Salacia* species. *J. Tradit. Med. 22*, 145–153.
11. Serasinghe, S., Serasinghe, P., Yamazaka, H., Nishiguchi, K., Hombhanje, F., Nakanishi, S., Sawa, K., Hattori, M., and Namba, T. (1990) Oral hypoglycaemic effect of *Salacia reticulata* in the streptozocotocin induced diabetic rat. *Phytother. Res. 4*, 205–206.
12. Shimoda, H., Fujimura, T., Makino, K., Yoshijima, K., Naitoh, K., Ihota, H., and Miwa, Y. (1999) Safety profile of extractive from trunk of *Salacia reticulata* (Celastraceae). *J. Food Hyg. Soc. Jpn. 20*, 198–205.
13. Jayawardena, M. H. S., de Alwis, N. M. W., Hettigoda, V., and Fernando, D. J. S. (2005) Double blind randomised placebo controlled cross over study of a herbal preparation containing *Salacia reticulata* in the treatment of type 2 diabetes. *J. Ethnopharmacol. 97*, 215–218.
14. Im, R., Mano, H., Nakatani, S., Shimizu, J., and Wada, M. (2008) Aqueous extract of *Kothala himbutu* (*Salacia reticulata*) stems promotes oxygen consumption and suppresses body fat accumulation in mice. *J. Health Sci. 54*, 645–653.
15. Muraoka, O., Xie, W., Tanabe, G., Amer, M. F. A., Minematsu, T., and Yoshikawa, M. (2008) On the structure of the bioactive constituent from Ayurvedic medicine *Salacia reticulata*: Revision of the literature. *Tetrahedron Lett. 49*, 7315–7317.
16. Yoshikawa, M., Murakami, T., Shimada, H., Matsuda, H., Yamahara, J., Tanabe, G., and Muraoka, O. (1997) Salacinol, potent antidiabetic principle with unique thiosugar sulfonium sulfate structure from the Ayurvedic traditional medicine *Salacia reticulata*. Sri Lanka and India. *Tetrahedron Lett. 38*, 8367–8370.
17. Yoshikawa, M., Murakami, T., Yashiro, K., and Matsuda, H. (1998) Kotalanol, a potent α-glucosidase inhibitor with thiosugar sulfonium sulfate structure, from antidiabetic ayurvedic medicine *Salacia reticulata*. *Chem. Pharm. Bull. 46*, 1339–1340.
18. Semenza, G., Auricchio, S., and Rubino, A. (1965) Multiplicity of human intestinal disaccharidases. I. Chromatographic separation of maltases and of two lactases. *Biochim. Biophys. Acta 96*, 487–497.
19. Semenza, G., Auricchio, S., and Mantei, N. (2001) in *The Metabolic Basis of Inherited Disease*, McGraw-Hill: New York.
20. Rossi, E. J., Sim, L., Kuntz, D. A., Hahn, D., Johnston, B. D., Ghavami, A., Szczepina, M. G., Kumar, N. S., Sterchi, E. E., Nichols, B. L., Pinto, B. M., and Rose, D. R. (2006) Inhibition of recombinant human maltase glucoamylase by salacinol and derivatives. *FEBS J. 273*, 2673–2683.
21. Nasi, R., Patrick, B. O., Sim, L., Rose, D. R., and Pinto, B. M. (2008) Studies directed toward the stereochemical structure determination of the naturally occurring glucosidase inhibitor, kotalanol: Synthesis and inhibitory activities against human maltase glucoamylase of seven-carbon, chain-extended homologues of salacinol. *J. Org. Chem. 73*, 6172–6181.
22. Mohan, S., and Pinto, B. M. (2007) Zwitterionic glycosidase inhibitors: Salacinol and related analogues. *Carbohydr. Res. 342*, 1551–1580.
23. Li, C., Begum, A., Numao, S., Park, K. H., Withers, S. G., and Brayer, G. D. (2005) Acarbose rearrangement mechanism implied by the kinetic and structural analysis of human pancreatic α-amylase in complex with analogues and their elongated counterparts. *Biochemistry 44*, 3347–3357.
24. Bischoff, H. (1994) Pharmacology of α-glucosidase inhibition. *Eur. J. Clin. Invest. 24* (Suppl. 3), 3–10.

25. Madar, Z. (1989) The effect of acarbose and miglitol (BAY-M-1099) on postprandial glucose levels following ingestion of various sources of starch by nondiabetic and streptozotocin-induced diabetic rats. *J. Nutr. 119*, 2023–2029.
26. Toeller, M. (1992) Nutritional recommendations for diabetic patients and treatment with α-glucosidase inhibitors. *Drugs 44* (Suppl. 3), 13–20.
27. Meckling, K. A. (2006) Nutrient Drug Interactions, CRC/Taylor & Francis, Boca Raton, FL.
28. Sim, L., Quezada-Calvillo, R., Sterchi, E. E., Nichols, B. L., and Rose, D. R. (2008) Human intestinal maltase-glucoamylase: Crystal structure of the N-terminal catalytic subunit and basis of inhibition and substrate specificity. *J. Mol. Biol. 375*, 782–792.
29. Johnston, B. D., Jensen, H. H., and Pinto, B. M. (2006) Synthesis of sulfonium sulfate analogues of disaccharides and their conversion to chain-extended homologues of salacinol: New glycosidase inhibitors. *J. Org. Chem. 71*, 1111–1118.
30. Jayakanthan, K., Mohan, S., and Pinto, B. M. (2009) Structure proof and synthesis of kotalanol and de-O-sulfonated kotalanol, glycosidase inhibitors isolated from an herbal remedy for the treatment of type-2 diabetes. *J. Am. Chem. Soc. 131*, 5621–5626.
31. Ghavami, A., Johnston, B. D., and Pinto, B. M. (2001) A new class of glycosidase inhibitor: Synthesis of salacinol and its stereoisomers. *J. Org. Chem. 66*, 2312–2317.
32. Otwinowski, Z., and Minor, W. (1997) Processing of X-ray diffraction data collected in oscillation mode. *Methods Enzymol. 276*, 307–326.
33. Murshudov, G. N., Vagin, A. A., and Dodson, E. J. (1997) Refinement of macromolecular structures by the maximum-likelihood method. *Acta Crystallogr. D53*, 240–255.
34. Emsley, P., and Cowtan, K. (2004) Coot: Model-building tools for molecular graphics. *Acta Crystallogr. D60*, 2126–2132.
35. Schuttelkopf, A. W., and van Aalten, D. M. (2004) PRODRG: A tool for high-throughput crystallography of protein-ligand complexes. *Acta Crystallogr. D60*, 1355–1363.
36. Perrakis, A., Harkiolaki, M., Wilson, K. S., and Lamzin, V. S. (2001) ARP/wARP and molecular replacement. *Acta Crystallogr. D57*, 1445–1450.
37. Nasi, R., Sim, L., Rose, D. R., and Pinto, B. M. (2007) New chain-extended analogues of salacinol and blintol and their glycosidase inhibitory activities. Mapping the active-site requirements of human maltase glucoamylase. *J. Org. Chem. 72*, 180–186.
38. Quezada-Calvillo, R., Sim, L., Ao, Z., Hamaker, B. R., Quaroni, A., Brayer, G. D., Sterchi, E. E., Robayo-Torres, C. C., Rose, D. R., and Nichols, B. L. (2008) Luminal starch substrate "brake" on maltase-glucoamylase activity is located within the glucoamylase subunit. *J. Nutr. 138*, 685–692.
39. Lovering, A. L., Lee, S. S., Kim, Y. W., Withers, S. G., and Strynadka, N. C. (2005) Mechanistic and structural analysis of a family 31 α-glycosidase and its glycosyl-enzyme intermediate. *J. Biol. Chem. 280*, 2105–2115.
40. Wen, X., Yuan, Y., Kuntz, D. A., Rose, D. R., and Pinto, B. M. (2005) A combined STD-NMR/molecular modeling protocol for predicting the binding modes of the glycosidase inhibitors kifunensine and salacinol to Golgi α-mannosidase II. *Biochemistry 44*, 6729–6737.
41. Vocadlo, D. J., and Davies, G. J. (2008) Mechanistic insights into glycosidase chemistry. *Curr. Opin. Chem. Biol. 12*, 539–555.
42. Withers, S. G., Namchuk, M., and Mosi, R. (1999) Potent glycosidase inhibitors: Transition state mimics or simply fortuitous binders? In Iminosugars as glycosidase inhibitors: Nojirimycin and beyond (Stuttz, A. E., Ed.) pp 188−203, Wiley-VCH, Weinheim, Germany.
43. Mosi, R., Sham, H., Uitdehaag, J. C., Ruiterkamp, R., Dijkstra, B. W., and Withers, S. G. (1998) Reassessment of acarbose as a transition state analogue inhibitor of cyclodextrin glycosyltransferase. *Biochemistry 37*, 17192–17198.
44. Berland, C. R., Sigurskjold, B. W., Stoffer, B., Frandsen, T. P., and Svensson, B. (1995) Thermodynamics of inhibitor binding to mutant forms of glucoamylase from *Aspergillus niger* determined by isothermal titration calorimetry. *Biochemistry 34*, 10153–10161.
45. Liu, H., Nasi, R., Jayakanthan, K., Sim, L., Heipel, H., Rose, D. R., and Pinto, B. M. (2007) New synthetic routes to chain-extended selenium, sulfur, and nitrogen analogues of the naturally occurring glucosidase inhibitor salacinol and their inhibitory activities against recombinant human maltase glucoamylase. *J. Org. Chem. 72*, 6562–6572.
46. Liu, H., Sim, L., Rose, D. R., and Pinto, B. M. (2006) A new class of glucosidase inhibitor: Analogues of the naturally occurring glucosidase inhibitor salacinol with different ring heteroatom substituents and acyclic chain extension. *J. Org. Chem. 71*, 3007–3013.
47. Chehade, J. M., and Mooradian, A. D. (2000) A rational approach to drug therapy of type 2 diabetes mellitus. *Drugs 60*, 95–113.